Lithium-Ion Batteries Hot Paper

International Edition: DOI: 10.1002/anie.201604554
German Edition: DOI: 10.1002/ange.201604554

Fluorine-Doped Antiperovskite Electrolyte for All-Solid-State Lithium-Ion Batteries

*Yutao Li[+], Weidong Zhou[+], Sen Xin, Shuai Li, Jinlong Zhu, Xujie Lü, Zhiming Cui, Quanxi Jia, Jianshi Zhou, Yusheng Zhao, and John B. Goodenough**

Abstract: *A fluorine-doped antiperovskite Li-ion conductor $Li_2(OH)X$ (X = Cl, Br) is shown to be a promising candidate for a solid electrolyte in an all-solid-state Li-ion rechargeable battery. Substitution of F^- for OH^- transforms orthorhombic Li_2OHCl to a room-temperature cubic phase, which shows electrochemical stability to 9 V versus Li^+/Li and two orders of magnitude higher Li-ion conductivity than that of orthorhombic Li_2OHCl. An all-solid-state $Li/LiFePO_4$ with F-doped Li_2OHCl as the solid electrolyte showed good cyclability and a high coulombic efficiency over 40 charge/discharge cycles.*

Interest in next generation Li-ion batteries with guaranteed safety has stimulated intensive work on solid Li-ion electrolytes for all-solid-state batteries and as separators for high-capacity batteries with redox-flow electrodes.[1–6] The electrolytes of today's commercial rechargeable Li-ion batteries consist of a mixture of organic solvents with a Li-ion salt; these electrolytes are flammable and have limited electrochemical windows, usually $E_g \leq 3.0$ V. In addition to greater safety, a solid Li-ion electrolyte that is chemically stable and wet on contact with metallic Li would enable use of a Li-metal anode without dendrite formation; and if it has a window that extends beyond 6 V, it would allow realization of a 5-V rechargeable cell.

Oxides with garnet, LISICON, and perovskite structures have been investigated as Li-ion solid electrolytes.[7–17] The garnet electrolyte has a huge interfacial resistance against a Li-metal anode; its surface is not wet by metallic lithium, and dendrites have penetrated garnet grain boundaries.[18,19] The commercial $Li_{1.3}Al_{0.3}Ti_{1.7}(PO_4)_3$ with the LISICON structure and the perovskite $Li_{3x}La_{2/3-x}TiO_3$ or $Li_{3/8}Sr_{7/16}M_{1/4}Ta_{3/4}O_3$ (M = Zr or Hf) are all reduced on contact with Li metal owing to the reduction of Ti^{IV} or Ta^{V}.[20,21] Of the non-oxide Li^+ electrolytes, the sulfide $Li_{10}GeP_2S_{12}$, although exhibiting a remarkably high Li-ion conductivity,[22] is not stable in an all-solid-state battery with a metallic Li anode and an oxide cathode.[23]

A report[24] of a Li-ion conductivity of 10^{-3} S cm^{-1} in the antiperovskite "Li_3OX" (X = Cl, Br) has stimulated interests in these structures as promising solid Li-ion electrolytes. However, subsequent studies of the Li^+ conductivity in crystalline "Li_3OX" compounds have reported room-temperature conductivities from 5×10^{-7} to 2×10^{-4} S cm^{-1},[24–27] with indications that the as-prepared "Li_3OX" may be Li_2OHX antiperovskite rather than Li_3OX. Herein, we report that replacing some of the OH^- by F^- is possible and that $Li_2(OH)_{0.9}F_{0.1}Cl$ is demonstrated to be a promising Li-ion solid electrolyte that is stable on contact with metallic Li and has an energy window extending to 9 V versus Li^+/Li.

The X-ray diffraction (XRD) patterns of the as-prepared "Li_3OBr" and Li_2OHBr samples as well as for those obtained by different water contents in the starting materials are shown in Figure 1 a. The assumed "Li_3OBr" sample was prepared, as has been reported, by firing LiOH and LiBr at 400 °C for

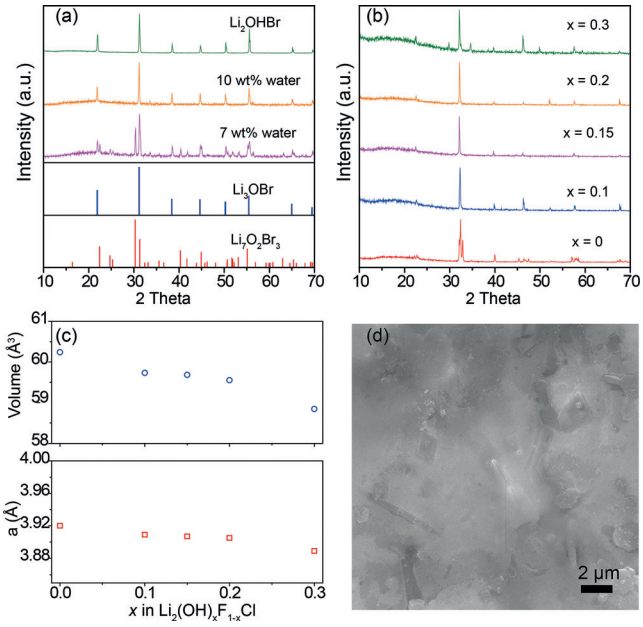

Figure 1. XRD patterns of a) Li_2OHBr, H-doped Li_3OBr with different water content and b) $Li_2(OH)_{1-x}F_xCl$, c) Lattice parameters and unit-cell volume of $Li_2(OH)_{1-x}F_xCl$, d) SEM image of $Li_2(OH)_{0.9}F_{0.1}Cl$.

[*] Dr. Y. Li,[+] Dr. W. Zhou,[+] Dr. S. Xin, Dr. Z. Cui, Prof. J. Zhou, Prof. J. B. Goodenough
Materials research program and the Texas Materials Institute, University of Texas at Austin
Austin, TX 78712 (USA)
E-mail: jgoodenough@mail.utexas.edu
Dr. S. Li, Dr. J. Zhu, Prof. Y. Zhao
High Pressure Science and Engineering Center, University of Nevada Las Vegas, NV 89154 (USA)
Dr. X. Lü, Prof. Q. Jia
Center for Integrated Nanotechnologies, Las Los Alamos National Laboratory
Los Alamos, NM 87545 (USA)
Dr. S. Xin
School of Chemistry and Chemical Engineering, Hefei University of Technology
Hefei, Anhui, 230009 (P.R. China)
[+] These authors contributed equally.

Supporting information for this article can be found under: http://dx.doi.org/10.1002/anie.201604554.

12 h.[24] We were unable to prepare "Li_3OBr" by directly melting dry LiOH and LiBr; the H^+ of LiOH is hard to be removed in the form of H_2O because of the strong O–H bond of the OH^- ion as has been reported for attempts to prepare Na_3OX from NaOH and NaX as the starting materials.[28] However, it is easy to obtain Li_2OHBr in 30 min at 350 °C from the following reaction in Equation (1):

$$LiBr + LiOH \rightarrow Li_2OHBr + H_2O \quad (1)$$

Moreover, dry Li_2O and LiX do not react at 350 °C or even at the higher temperatures of 500–600 °C; and calculation shows that Li_3OCl has a positive formation energy relative to a two-phase mixture of LiCl and Li_2O.[29] We found the reaction of dry Li_2O and LiX depends on the amount of water added to the starting materials. With less than 10 wt % water, a multiphase product containing Li_2OHBr and layered $Li_7O_2Br_3$ were formed, Figure 1 a. The colors of the products with and without water fired at high temperatures are white and black, respectively (Figure S1). The lattice parameters of cubic $Li_{3-x}OH_xX$ (X = Cl and Br) decreases as the H^+ concentration x increases.[30] The reported "Li_3OBr" and Li_2OHBr have the same lattice parameter $a = 4.056$ Å; so "Li_3OBr" and Li_2OHBr may have very close hydrogen content. The only exception is a LiBr-deficient sample reported by Zhao and Daemen,[24] which has a smaller lattice parameter 4.02 Å and a higher Li-ion conductivity of 10^{-3} S cm^{-1}. A Fourier Transform Infrared Spectrum of "Li_3OBr" shows a peak at 3200–3600 cm^{-1} (Figure S2), which corresponds to the stretching vibration of OH^-. The protons replace a Li^+ of the antiperovskite structure in Li_2OHBr. Pure cubic "Li_3OBr" and Li_2OHBr samples were obtained as well by aliovalent cation doping, high-energy ball-milling, or liquid-N_2 quenching; each sample showed a low Li-ion conductivity of 10^{-6} S cm^{-1} at room temperature (Figures S3 and S4). Figure 1 b shows XRD patterns for $Li_2(OH)_{1-x}F_xCl$ ($x = 0$–0.3) obtained with LiOH, LiCl, and LiF as the starting materials. Both the cubic lattice parameter and cell volume of $Li_2(OH)_{1-x}F_xCl$ decrease progressively with F^- content (Figure 1 c), which is caused by the different values of ionic radii of F^- (1.33 Å) and $(OH)^-$ (1.37 Å) ions. The F^- and X^- elements were evenly distributed in $Li_2(OH)_{0.9}F_{0.1}Cl$ (Figure S5) and Li_2OHBr (Figure S6). Almost 100 %-dense $Li_2(OH)_{0.9}F_{0.1}Cl$ pellets were prepared at 350 °C in 30 min, Figure 1 d. In contrast to this simple, low-cost synthesis, which is suitable for large-scale production, the preparation of other ceramic Li^+ electrolytes require sintering for long times at high temperature with several intermediate grindings. Moreover, a special firing technique such as spark plasma sintering or hot-pressing may be required to obtain a high-density ceramic Li^+-electrolyte pellet.

The substitution of F^- for OH^- also increases the cubic antiperovskite tolerance factor for "Li_3OX" [Eq. (2)]:

$$t = (X\text{–}Li)/\left(\sqrt{2}(O - Li)\right) \quad (2)$$

where X-Li and O-Li are the equilibrium bond lengths. Increasing t to over 0.9 stabilizes the cubic phase. A $t = 0.85$ and 0.91 for X = Cl and Br, respectively, is obtained with Shannon tabulated ionic radii; the size of Br^- is larger than Cl^- for the A site in the antiperovskite structure. With a $t = 0.85$, Li_3OCl should be distorted to a lower symmetry, and its cubic form is dynamically unstable with respect to cooperative Li_6O octahedral rotations; and Li_2OHCl and Li_2OHBr have, respectively, room-temperature orthorhombic and cubic structures. Increasing t by F^- substitution for OH^- makes $Li_2(OH)_{0.9}F_{0.1}Cl$ cubic at room temperatures, hereby favoring a disordering of the OH^- orientation.

The crystal structure of cubic Li_2OHCl as determined by neutron diffraction[31] is shown in Figure 2 a; the Li vacancies

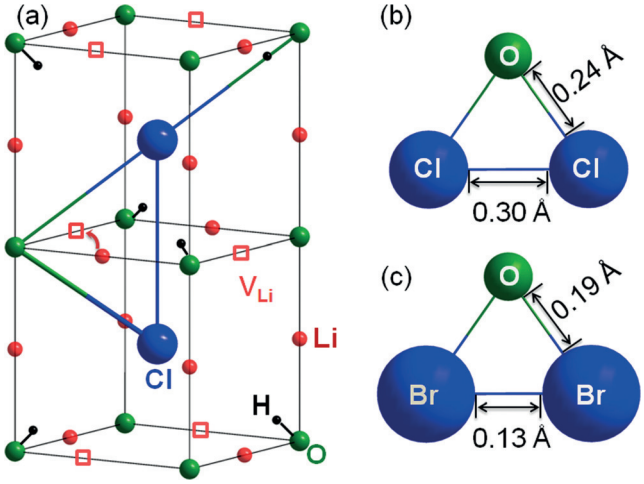

Figure 2. a) Crystal structure of cubic Li_2OHCl; H^+ is on the axis of a O–Cl bond and forms an OH^- bond; the triangle is the Cl-O-Cl plane in the path of Li-ion transport. Red open squares indicate Li vacancies. b),c) The size of the Cl-O-Cl triangle in cubic Li_2OHCl and the Br-O-Br triangle in Li_2OHBr or "Li_3OBr".

are ordered to make each oxide ion coordinated by 4 Li^+ and 2 H^+ cations. The Li^+ ions form 180° O–Li–O bonds in the cubic phase and the H^+ ions are displaced from a cubic edge to form linear O–H–Cl bonds in Li_2OHCl and bent O–H–Br bonds in Li_2OHBr because of the larger size of the Br^- ions. A Li^+ jump to a Li^+ vacancy is through a triangular $O^{2-}(X)^-_2$ site (see Figure 2 b,c); the Li^+ jump is hindered by the coulomb repulsion and steric hindrance of the H^+ ions with a fixed O–H–X hydrogen bond. An abrupt change of the Li^+ conductivity from 10^{-8} to 10^{-5} S cm^{-1} of Li_2OHCl at an orthorhombic to cubic transition near 35 °C indicates that a random orientation of the hydrogen bond to one of its 8 nearest-neighbor X^- ions in the cubic structure facilitates rotations of the hydrogen bonds to lower the activation energy for a Li^+ jump to a neighboring Li-site vacancy. Substitution of F^- for an OH^- anion not only reduces the number of hindering H^+ ions, but also stabilizes the more favorable cubic phase at room temperature.

The room-temperature conductivity data for cubic $Li_2(OH)_{1-x}F_xCl$ with $x = 0.1$ and 0.15 shown in Figure 3 a exhibits a low-frequency tail characteristic of electrode blocking of mobile ions. The impedance plot is fit with the conventional equivalent circuit shown in the insert of Figure 3 a. The

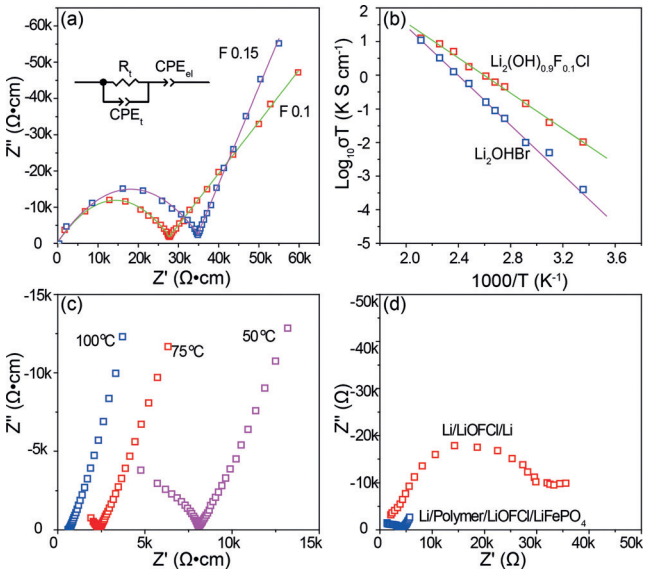

Figure 3. a) The impedance plots of $Li_2(OH)_{1-x}F_xCl$ at 25 °C. Inset: equivalent circuit. b) Temperature dependence of the Li-ion conductivity of Li_2OHBr and $Li_2(OH)_{0.9}F_{0.1}Cl$. c) The impedance plots of $Li_2(OH)_{1-x}F_xCl$ at high temperature. d) The impedance plots of the cell with and without polymer electrolyte.

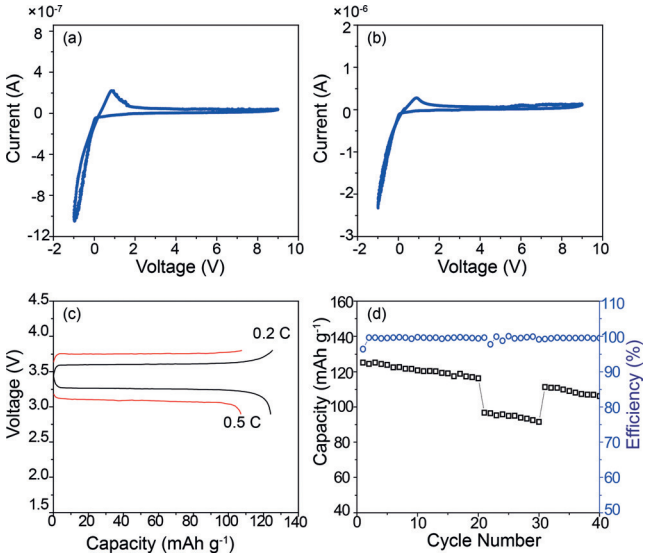

Figure 4. A cyclic voltammogram of a) $Li_2(OH)_{0.9}F_{0.1}Cl$ and b) Li_2OHBr at a scanning rate of 0.5 $mV s^{-1}$. c) Charge and discharge voltage profiles and d) cycling performance at 0.2 C of a Li/$LiFePO_4$ all-solid-state battery at 65 °C with $Li_2(OH)_{0.9}F_{0.1}Cl$ as the solid electrolyte.

measured Li^+ conductivities of 3.5×10^{-5} $S cm^{-1}$ at 25 °C agrees well with prediction from ab initio molecular dynamics (AIMD) simulations made with a combination of percolation theory and first-principles calculations;[32] it is about 2 orders of magnitude lower than that originally reported by Zhao; it is also a little lower than that of garnet and LISICON-structured oxide electrolytes. The Arrhenius plot of Figure 3b over 298–430 K gives activation energies of 0.52 and 0.75 eV, respectively, for $Li_2(OH)_{0.9}F_{0.1}Cl$ and Li_2OHBr. $Li_2(OH)_{0.9}F_{0.1}Cl$ exhibited a high Li-ion conductivity of 1.9×10^{-3} $S cm^{-1}$ at 100 °C (Figure 3c). The higher activation energy in Li_2OHBr resulted from the larger size of Br ions, which squeezes the Li-ion transport channel. Larger size anions (Br^- or I^-) in the 12-coordinated X sites will significantly hinder the Li-ion movement inside the antiperovskite framework, while a LiX deficiency of Li_2OHX other than by a aliovalent cation doping might be more efficient to lower further the activation energy of Li-ion transport and increase Li-ion conductivity.

The cyclic voltammograms of $Li_2(OH)_{0.9}F_{0.1}Cl$ and Li_2OHBr are shown in Figure 4a,b. The small peak in the initial anodic sweep near 0 V corresponds to the reduction of $Li_2(OH)_{0.9}F_{0.1}Cl$ by Li insertion at the surface of the electrolyte to form a passivating interface layer that enables using a melting metallic Li anode in Li rechargeable battery with $Li_2(OH)_{0.9}F_{0.1}Cl$ or Li_2OHCl electrolyte at 190 °C;[27] but a Li dendrite can still penetrate $Li_2(OH)_{0.9}F_{0.1}Cl$ or Li_2OHCl electrolyte and short-circuit the cell at 65 °C (Figure S1). There were no other oxidation/reduction peaks to 9 V. The protons inside the electrolyte are strongly attached to the oxygen and their movements should, therefore, be limited to rotations of the $(OH)^-$ anion. The "Li_3OCl" has been reported to decompose into Li_2O_2, LiCl, and $LiClO_4$ above an applied voltage of 2.5 V. Replacement of Li^+ by H^+ appears to have stabilized a metastable "Li_3OCl" to a stable Li_2OHCl. The antiperovskite materials are very hydroscopic; the room-temperature Li-ion conductivities of the antiperovskite materials increase several orders of magnitude and they are unstable at high voltages above 3 V after they absorb the water in air. For example, the room-temperature conductivity of $Li_2(OH)_{0.9}F_{0.1}Cl$ from EIS increased from 10^{-5} to 10^{-2} $S cm^{-1}$ after the $Li_2(OH)_{0.9}F_{0.1}Cl$ powders were exposed to air for 10 seconds; the conductivity increase may be from the fast proton movement inside the pellet. The cyclic voltammetry of Li/water-contaminated $Li_2(OH)_{0.9}F_{0.1}Cl$/Au cell showed that $Li_2(OH)_{0.9}F_{0.1}Cl$ was unstable at voltages above 2 V after the $Li_2(OH)_{0.9}F_{0.1}Cl$ powders were contaminated by moisture (Figure S7).

To confirm that Li^+ is the mobile ion in $Li_2(OH)_{0.9}F_{0.1}Cl$ and to test the performance of the electrolyte, we fabricated a $LiFePO_4$/Li all-solid-state cell in which the $LiFePO_4$ cathode was embedded in a Li^+-conductive polymer membrane containing a polymer binder and an electronic conductor carbon black in a loading of 5 $mg cm^{-2}$. The Li-metal anode and $Li_2(OH)_{0.9}F_{0.1}Cl$ electrolyte were separated by the Li^+-conducting polymer membrane (100 μm thick with $\sigma_{Li}=10^{-4}$ $S cm^{-1}$ at 65 °C), which significantly reduced the interfacial resistance of the cell and suppressed any Li-dendrite growth (Figure 3d); the polymer membrane is also stable up to 4.7 V at 65 °C (Figure S8). Figure 4c shows the charge/discharge voltage profiles at 0.2 and 0.5 C at 65 °C; no irreversible capacity loss is observed in the initial cycle since the Li-metal/electrolyte interphase formed during assembly contains Li^+ from the anode. It shows an initial discharge capacity of 125 and 108 $mAh g^{-1}$ at 0.2 and 0.5 C, respectively. The capacity is retained at 120 $mAh g^{-1}$ during the initial 15 cycles at 0.2 C with a coulombic efficiency of 99 ± 0.5 % over 40 cycles, which indicates that the electrode/electrolyte interfaces are stable with cycling at 65 °C (Figure 4d). Metallic Li wets the polymer electrolyte surface in the formation of the anode/electrolyte interface phase.

In summary, we have shown that the antiperovskite Li_2OHX, X = Cl or Br, phase can be doped by the substitution of OH^- by F^- to provide an acceptable Li-ion electrolyte for an all-solid-state high-voltage rechargeable battery. The relatively simple preparation process and outstanding electrochemical stability of $Li_2(OH)_{0.9}F_{0.1}Cl$ make it a promising candidate electrolyte for all-solid-state batteries.

Acknowledgements

This work was supported by the ARPA-E project (0670-3052).

Keywords: all-solid-state battery · antiperovskite · lithium-ion battery · solid electrolyte

How to cite: *Angew. Chem. Int. Ed.* **2016**, *55*, 9965–9968
Angew. Chem. **2016**, *128*, 10119–10122

[1] J. B. Goodenough, Y. Kim, *Chem. Mater.* **2010**, *22*, 587–603.
[2] Y. Zhao, D. Yu, Y. Li, L. Peng, H. R. Byon, J. B. Goodenough, G. Yu, *Chem. Soc. Rev.* **2015**, *44*, 7968–7996.
[3] J. B. Goodenough, K. S. Park, *J. Am. Chem. Soc.* **2013**, *135*, 1167–1176.
[4] P. G. Bruce, S. A. Freunberger, L. J. Hardwick, J.-M. Tarascon, *Nat. Mater.* **2012**, *11*, 19–29.
[5] Y. Kato, S. Hori, T. Saito, K. Suzuki, M. Hirayama, A. Mitsui, M. Yonemura, H. Iba, R. Kanno, *Nat. Energy* **2016**, *1*, 16030.
[6] Y. Wang, W. Davidson Richards, S. P. Ong, L. J. Miara, J. C. Kim, Y. Mo, G. Ceder, *Nat. Mater.* **2015**, *14*, 1026–1031.
[7] R. Murugan, V. Thangadurai, W. Weppner, *Angew. Chem. Int. Ed.* **2007**, *46*, 7778–7781; *Angew. Chem.* **2007**, *119*, 7925–7928.
[8] H. Aono, E. Sugimoto, Y. Sadaaka, N. Imanaka, G. Y. Adachi, *J. Electrochem. Soc.* **1989**, *136*, 590–591.
[9] S. Stramare, V. Thangadurai, W. Weppner, *Chem. Mater.* **2003**, *15*, 3974–3990.
[10] V. Thangadurai, S. Narayanan, D. Pinzaru, *Chem. Soc. Rev.* **2014**, *43*, 4714–4727.
[11] G. Adachi, N. Imanaka, H. Aono, *Adv. Mater.* **1996**, *8*, 127–135.
[12] J. A. Alonso, J. Sanz, J. Santamaría, C. León, A. Várez, M. T. Fernández-Díaz, *Angew. Chem. Int. Ed.* **2000**, *39*, 619–621; *Angew. Chem.* **2000**, *112*, 633–635.
[13] C. Ma, K. Chen, C. Liang, C.-W. Nan, R. Ishikawa, K. More, M. Chi, *Energy Environ. Sci.* **2014**, *7*, 1638–1642.
[14] Z. Liu, W. Fu, E. A. Payzant, X. Yu, Z. Wu, N. J. Dudney, J. Kiggans, K. Hong, A. J. Rondinone, C. Liang, *J. Am. Chem. Soc.* **2013**, *135*, 975–978.
[15] E. Rangasamy, J. Wolfenstine, J. Sakamoto, *Solid State Ionics* **2012**, *206*, 28–32.
[16] S. Ohta, T. Kobayashi, T. Asaoka, *J. Power Sources* **2011**, *196*, 3342–3345.
[17] Y. Shimonishi, A. Toda, T. Zhang, A. Hirano, N. Imanishi, O. Yamamoto, Y. Takeda, *Solid State Ionics* **2011**, *183*, 48–53.
[18] Y. Li, J. T. Han, C. A. Wang, H. Xie, J. B. Goodenough, *J. Mater. Chem.* **2012**, *22*, 15357–15361.
[19] Y. Ren, Y. Ren, Y. Lin, C. W. Nan, *Electrochem. Commun.* **2015**, *57*, 27–30.
[20] C. H. Chen, S. Xie, E. Sperling, A. S. Yang, G. Henriksen, K. Amine, *Solid State Ionics* **2004**, *167*, 263–272.
[21] B. Huang, Y. Li, S. W. Zhong, *ACS Appl. Mater. Interfaces* **2016**, DOI: 10.1021/acsami.6b03070.
[22] N. Kamaya, K. Homma, Y. Yamakawa, M. Hirayama, R. Kanno, M. Yonemura, T. Kamiyama, Y. Kato, S. Hama, K. Kawamoto, A. Mitsui, *Nat. Mater.* **2011**, *10*, 682–686.
[23] A. C. Luntz, J. Voss, K. Reuter, *J. Phys. Chem. Lett.* **2015**, *6*, 4599–4604.
[24] Y. Zhao, L. L. Daemen, *J. Am. Chem. Soc.* **2012**, *134*, 15042–15047.
[25] S. Li, J. Zhu, Y. Wang, J. W. Howard, X. X. Lü, Y. Li, R. S. Kumara, L. Wang, L. L. Daemen, Y. Zhao, *Solid State Ionics* **2016**, *284*, 14–19.
[26] X. Lü, J. W. Howard, A. Chen, J. Zhu, S. Li, G. Wu, P. Dowden, H. Xu, Y. Zhao, Q. Jia, *Adv. Sci.* **2016**, *3*, 1500359.
[27] Z. D. Hood, H. Wang, A. S. Pandian, J. K. Keum, C. Liang, *J. Am. Chem. Soc.* **2016**, *138*, 1768–1771.
[28] Y. Wang, Q. Wang, Z. Liu, Z. Zhou, S. Li, J. Zhu, R. Zou, Y. Wang, J. Lin, Y. Zhao, *J. Power Sources* **2015**, *293*, 735–740.
[29] A. Emly, E. Kioupakis, A. Van der Ven, *Chem. Mater.* **2013**, *25*, 4663–4670.
[30] G. Schwering, A. Hönnerscheid, L. van Wüllen, M. Jansen, *ChemPhysChem* **2003**, *4*, 343–348.
[31] C. Eilbracht, W. Kockelmann, D. Hohlwein, H. Jacobs, *Physica B + C* **1997**, *234–236*, 48–50.
[32] Z. Deng, B. Radhakrishnan, S. P. Ong, *Chem. Mater.* **2015**, *27*, 3749–3755.

Received: May 10, 2016
Published online: June 30, 2016

